Food Chemistry: X 13 (2022) 100251

Contents lists available at ScienceDirect

Food Chemistry: X

journal homepage: www.sciencedirect.com/journal/food-chemistry-x

Sulfated heteropolysaccharides from *Undaria pinnatifida*: Structural characterization and transcript-metabolite profiling of immunostimulatory effects on RAW264.7 cells

Lihong Yang [a,b,1], Jun Liu [c,1], Xuewei Xia [b], Io Nam Wong [d], Sookja Kim Chung [d], Baojun Xu [e], Hesham R. El-Seedi [f], Bin Wang [a,*], Riming Huang [b,*]

[a] Shenzhen Hospital of Integrated Traditional Chinese and Western Medicine, Shenzhen 518104, China
[b] Guangdong Provincial Key Laboratory of Food Quality and Safety, College of Food Science, South China Agricultural University, Guangzhou 510642, China
[c] Laboratory of Pathogenic Biology, Guangdong Medical University, Zhanjiang 524023, China
[d] Faculty of Medicine, Macau University of Science and Technology, Macau, China
[e] Food Science and Technology Program, BNU-HKBU United International College, Zhuhai 519087, China
[f] Pharmacognosy Group, Department of Pharmaceutical Biosciences, Biomedical Centre, Uppsala University, Uppsala, Box 591, SE 751 24, Sweden

ARTICLE INFO

Keywords:
Undaria pinnatifida
Polysaccharide
Structural characterization
Immunostimulatory
Transcriptome
Metabolome

ABSTRACT

Investigation of the polysaccharides from an edible marine brown algae *Undaria pinnatifida* has led to obtaining three fractional sulfated polysaccharides UPPs 1–3 with molecular weights of 7.212 kDa, 13.924 kDa, and 55.875 kDa, respectively. All UPPs are composed of galactose, xylose, glucose, mannose, glucuronic acid, and mannuronic acid, while UPP-3 also consisted of fucose, arabinose, and fructose. The immunostimulatory assay revealed that UPP-3 had important effects on cell viability, nitric oxide levels, and secretion of cytokines TNF-α and IL-6 in RAW264.7 cells. Furthermore, the transcript-metabolite data along with western blot and immunofluorescent staining revealed that UPP-3 could stimulate the Toll-like receptor (TLR4) associated with the nuclear factor kappa-B (NF-κB) p65 signaling pathway of RAW264.7 cells. These findings of the immunomodulatory sulfated polysaccharide will provide a basic understanding to further exploitation of *U. pinnatifida* polysaccharides.

Introduction

Natural sulfated polysaccharides as the main biological components have been found in various organisms, such as animals, plants, and invertebrates (Gao et al., 2020). In recent years, many algal sulfated polysaccharides have gained much attention for the development of functional foods, pharmaceuticals, and cosmetics (Gurpilhares, Cinelli, Simas, Pessoa & Sette, 2019) due to their significantly pharmacological properties. For example, the green algae *Ulva pertusa* polysaccharide possessed an immunomodulatory effect (Gao et al., 2019). Red algae *Gracilaria rubra* polysaccharide exhibited antioxidant activity (Tong, Guijie, Yi, Shiyi, Xiaoxiong & Hong, 2017). Brown seaweed *Sargassum henslowianum* polysaccharide presented antiviral activity (Sun et al., 2020). An *S. tenerrimum* sulfated polysaccharide induced reactive oxygen species production (Raguraman et al., 2019). The fucoidan from brown algae *Padina boryana* showed antitumor activity (Usoltseva et al., 2018), and an *Ulva rigida* sulfated presented anticoagulant property (Adrien, Bonnet, Dufour, Baudouin, Maugard & Bridiau, 2019). Usually, the structures of these natural biological polysaccharides are diversified, including molecular weights, monosaccharide residue ratios, sulfate contents, and glycosidic linkage properties (Xu, Huang & Cheong, 2017), and these structural characteristics are fundamental to the biological activity of polysaccharides (Qiu et al., 2022). Thus, it is also necessary to clarify these bioactive polysaccharide structures related to their bioactivities.

Undaria pinnatifida, a kind of edible brown algae (Gudiel-Urbano and Goñi, 2002), is the source of sulfated polysaccharides with numerous biological activities (Wang, Park, Jeon, & Ryu, 2018). Such as immunostimulatory activity (Yu et al., 2019), anti-diabetic effects (Sim, Shin & Kim, 2019), antioxidant activity (Koh, Lu & Zhou, 2019), anti-

* Corresponding authors.
E-mail addresses: wangbin@szszxyjhyy.wecom.work (B. Wang), huangriming@scau.edu.cn (R. Huang).
[1] These authors equally contributed to this work.

https://doi.org/10.1016/j.fochx.2022.100251
Received 31 December 2021; Received in revised form 25 January 2022; Accepted 5 February 2022
Available online 9 February 2022

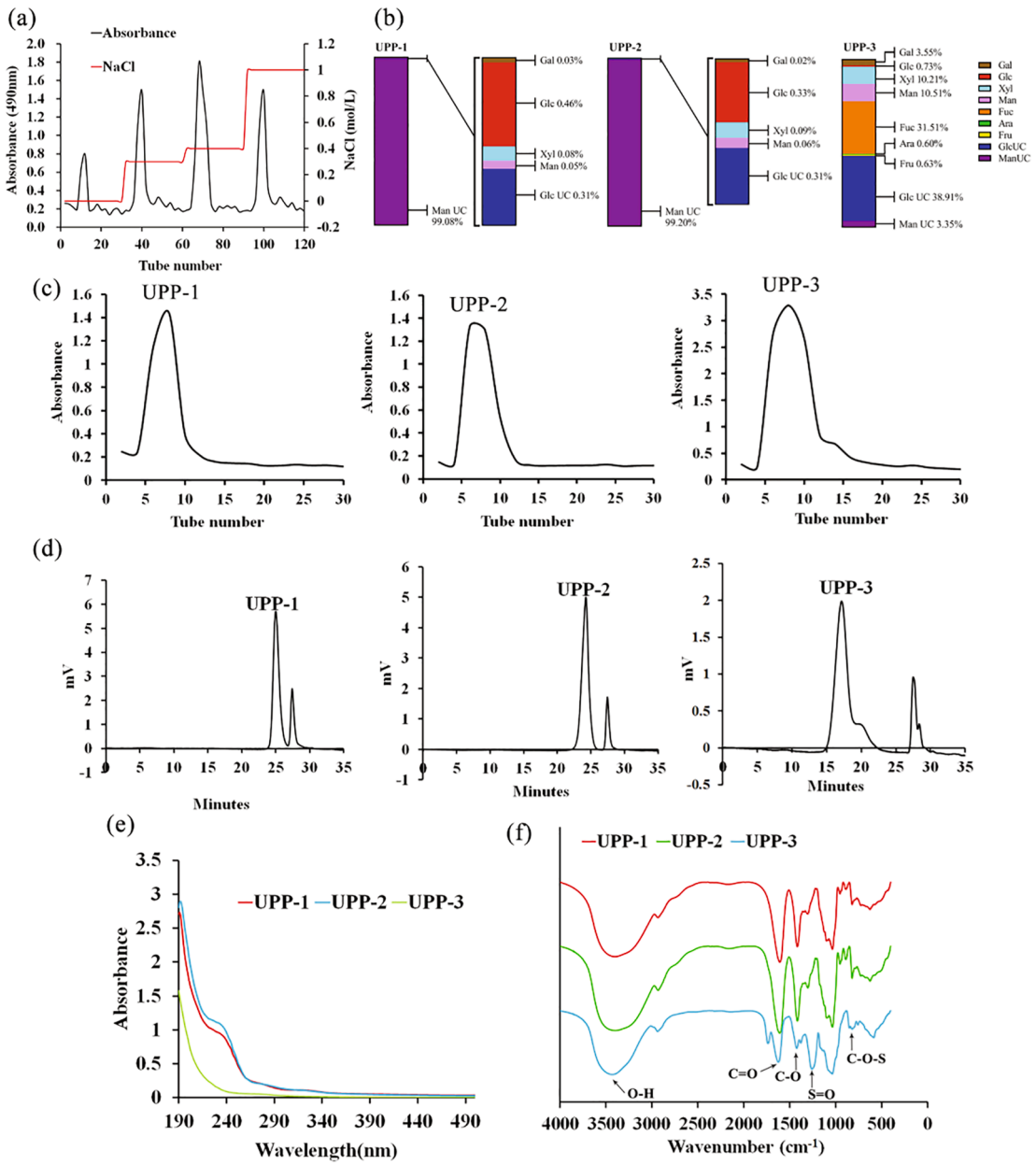

Fig. 1. (a) DEAE-sepharose fast flow chromatographic characteristic of UPPs 1–3. (b) The monosaccharide composition of UPPs 1–3. (c) Elution curve of UPPs 1–3 Sephadex G-100 column. (d) HPGPC data of UPPs 1–3. (e) UV spectra of UPPs 1–3. (f) FT-IR spectrum of UPPs 1–3.

metastasis effect (Wang et al., 2014), antiviral activity (Lee, Hayashi, Hashimoto, Nakano & Hayashi, 2004), and anticancer effect (Bovet, Samer & Daali, 2019). However, in some investigations of the immune-stimulatory effects of *U. pinnatifida* sulfated polysaccharides (Yu et al., 2019) the molecular details of their immune-stimulatory effects are still absent. Thus, the molecular features of immune-stimulatory sulfated polysaccharides from *U. pinnatifida* are needed to understand better for its further exploration.

This study was aimed to focus on the structural characterization of these sulfated polysaccharides from *U. pinnatifida*, their immune-stimulatory effects, including the cytotoxicity assay of macrophage, phagocytic activity, the production of nitric oxide (NO), the secretion of cytokines, mRNA expression of the cytokines inducible nitric oxide synthase (iNOS), tumor necrosis factor-α (TNF-α), and interleukin-6 (IL-6), and the molecular details of these immune-stimulatory effects revealed by the transcript-metabolite profiling combined with western blot and immunofluorescent staining. Therefore, the achievements of this study will give basic scientific data including structural characterization, cytokines of immune-stimulatory effects, and molecular details of transcription and metabolism for further exploitation of *U. pinnatifida* polysaccharides.

Materials and methods

Materials

Rongcheng City Aquatic Products Co. LTD (China) provided the air-dried *U. pinnatifida* powders, in September 2019. Shanghai Solarbio Bio-Technology Co. LTD (Shanghai, China) provided lipopolysaccharide (LPS), Sephadex G-100, and DEAE-Sepharose Fast Flow. Sigma Co. (NY, MO, U.S.A.) provided mannose (Man), arabinose (Ara), glucose (Glc), ribose (Rib), galactose (Gal), fucose (Fuc), xylose (Xyl), mannuronic acid (ManUA), glucuronic acid (GlcUA), and fructose (Fru), galacturonic acid (GalUA). The murine macrophage RAW264.7 cell lines were provided

by Jinan University in Guangzhou, China. Fetal bovine serum (FBS), penicillin–streptomycin, Dulbecco Modified Eagle Medium (DMEM), and phosphate buffer solution (PBS), were purchased from Gibco Life Technologies (Grand Island, NY, U.S.A.). Beijing Beyotime Biotechnology Co. LTD (China) provided NO kits, and Shanghai Bioss Biotechnology Co. LTD (China) provided the cell counting Kit-8 (CCK-8) kits. NeoBioscience Biotechnology Co. LTD (Shenzhen, China) provided the interleukin (IL)-6 kits and tumor necrosis factor (TNF)-α kits. All other chemical reagents used are analytical grade in the study.

Preparation of U. Pinnatifida polysaccharides

The air-dried *U. pinnatifida* powders (100 g) were used to extract the crude polysaccharides (UPP) based on the method in our reported data (Hao et al., 2019). 10 mL UPP (40 mg/mL) was subjected to a pre-equilibrated DEAE-Sepharose fast flow ion exchange column (3 × 70 cm) and continuously eluted with NaCl aqueous solutions (0, 0.3, 0.4, and 1.0 M) at a 0.5 mL/min flow rate. The collection of each 10 mL eluent was detected based on the phenol–sulfuric acid method. Three main elute fractions were illustrated in the elution curve (Fig. 1a), The obtained UPPs 1–3 were eluted by 0.3 M, 0.4 M, and 1.0 M NaCl aqueous solutions, respectively. The resultant UPPs 1–3 solutions were concentrated in vacuum, dialyzed, and freeze-dried, respectively. The total carbohydrate contents of the three fractions UPPs 1–3 were measured according to the phenol–sulfuric acid method (Masuko, Minami, Iwasaki, Majima, Nishimura & Lee, 2005) with D-glucose as the standard. Glucuronic uronic acid content was measured using an *m*-hydroxydiphenyl sulfuric-acid method (Masuko et al., 2005), with galacturonic acid as the standard. The protein contents were carried out based on Bradford's method (Bradford, 1976). The sulfate contents were determined based on the barium chloride-gelatin method (DODGSON & PRICE, 1962). The standard curve to determine the above contents of polysaccharides was shown in Fig. S1.

Monosaccharide compositions analysis

The monosaccharide composition of UPPs 1–3 was measured based on the method reported previously. In brief, 5 mg of each sample (UPPs 1–3) in 1 mL of 2.5 M trifluoroacetic acid (TFA) was hydrolyzed at 121 °C for 2 h in a sealed ampule. The hydrolysate was analyzed by ICS-5000 ion chromatography (ThermoFisher Scientific, MA, U.S.A.) coupled with Dionex™ CarboPac™ PA20 column (150 mm × 3 mm, 6.5 μm) and an electrochemical detector. The monosaccharide compositions were authenticated by comparison with the standards' retention times. The quantitative analysis of each monosaccharide was conducted based on the linear regression equation.

Molecular weights (MW) determination

The MW was measured by the high-performance gel-permeation chromatography (HPGPC) method previously reported in our study (Hao et al., 2019). The determination was performed on a Waters 1525 HPLC instrument equipped with a Waters 2414 differential refractive index detector and a TSK G-5000 PWXL column (7.8 mm × 300 mm), and a TSK G-3000 PWXL column (7.8 mm × 300 mm) in series. Each 10 μL UPPs 1–3 (3 mg/mL) was filtered by a 0.45 μm microporous filter and was subjected to the HPGPC column maintained at 35 °C, and then eluted with 0.02 M KH_2PO_4 aqueous solutions at a 0.6 mL/min flow rate. The various dextrans with different MWs (eight standards of 1 × 10^3-1 × 10^7 Da) as the standard were applied to establish the calibration curve.

UV analysis

The UV absorption (the wavelength range of 190–400 nm) of UPPs 1–3 (1 mg of each) was analyzed based on an Evolution 300 UV–VIS spectrometer (ThermoFisher Scientific, MA, U.S.A.) compared with the blank control (distilled water).

FT-IR analysis

The Fourier-transform infrared spectroscopy (FT-IR) analysis of UPPs (each, 1 mg) mixed with potassium bromide powder (spectroscopic grade) at a range of 4000–400 cm^{-1} was performed on an FT-IR spectrophotometer (VERTEX 70, Germany Bruker).

Molecular morphological determination

The microstructures of UPPs 1–3 were performed according to the method in our previously reported literature (Han et al., 2021). UPPs 1–3 (each 5 mg) were placed on a specimen holder with the help of double-sided adhesive tapes and coated with gold powder by vacuum coating apparatus. The character of UPPs 1–3 was observed at an accelerating potential of 15 kV during micrography with magnifications of 500 ×, 1000 ×, and 2000 × .

Triple-helix conformation

The triple-helix structures of UPPs 1–3 were carried out based on the Congo red method in the previously reported literature (Cao, Huang, Zhang, Li & Fu, 2018). UPPs 1–3 (each 5 mg) was solved in 10 mL distilled water, and 2 mL of UPPs aqueous solution was added 2 mL 50 μmol/L Congo red reagent thoroughly. The mixture was gradually adjusted to different NaOH concentrations (0, 0.10, 0.20, 0.25, 0.30, 0.40, and 0.50 mol/L) with 1 mol/L NaOH solution. The maximum absorption wavelength of the mixture was measured using ultraviolet scanning (200–700 nm), compared to the controls of laminarin and curdlan with a typical triple-helix conformation.

Immunomodulatory properties

Cell culture

The macrophage RAW264.7 cell lines were cultured in DMEM supplemented with a mixture of 1% (*v/v*) penicillin–streptomycin and 10% (*v/v*) FBS in an incubator at 37 °C with 5% CO_2.

Cytotoxicity test

The viability of macrophage RAW264.7 cell lines treated with UPPs 1–3 was measured *via* a CCK-8 assay. Briefly, 100 μL/well of RAW264.7 cells (about 3.0 × 10^4 cells/mL) seeded in a 96-well plate were incubated in a 5% CO_2 humidified incubator, at 37 °C for 24 h. The cell lines were completely washed with PBS solution and cultivated with 100 μL UPPs 1–3 aqueous solution with different concentrations ranging from 0 to 1000 μg/mL. CCK-8 solution (10 μL) was added to per well after another 24-hour incubation at 37 °C, and then the absorbance at 450 nm was carried out using a microplate reader (Model 550, Bio-Rad, CA, U.S.A.).

Assay of phagocytosis

The phagocytosis of macrophage RAW264.7 cell lines treated with UPPs were measured through the neutral red uptake method in our previously reported literature (Han, Hao, Yang, Chen, Wen & Huang, 2019). In brief, 100 μL/well of macrophage RAW264.7 cells (3.0 × 10^4 cells/mL) were cultivated in a 37 °C humidified incubator with 5% CO_2 for 24 h. After the incubation with 100 μL of UPPs 1–3 aqueous solution with various concentrations ranged from 0 to 1000 μg/mL for 24 h with 1 μg/mL LPS solution as a positive control, neutral red solution (100 μL/well of 0.5 mg/mL) was appended after the cultured medium removed. After a 1-hour incubation, the extra neutral red was removed using 0.01 M PBS (pH = 7.4) solution, and 100 μL/well lysis (ethanol/acetic acid = 1:1) solutions, and then lysed at room temperature for 12 h. After the lysis, the absorbance at 540 nm was recorded on a microplate reader

(Model 550, Bio-Rad, CA, U.S.A.).

Measurement of NO and cytokines

Macrophage RAW264.7 cell lines (5.0×10^5 cells/mL) in 24-well plate (500 μL/well) treated with 100 μL of UPPs 1–3 solutions (12.5, 25, 50, and 100 μg/mL) or LPS (0.1 μg/mL) solution, and incubated in a 37 °C 5% CO_2 humidified incubator for 24 h. After 24 h culture, the supernatants of RAW264.7 cells were collected, and the concentrations of NO, IL-6, and TNF-α were determined based on the manufacturer's instructions of ELISA kits.

RT-qPCR analysis

A concentration of 5×10^8 macrophages RAW264.7 cells/well on 6-well plates was cultivated for 24 h and was treated by 0 and 100 μg/mL of UPP-3 aqueous solutions. After 24 h, the total RNA of the cells was extracted with TRIzol™ reagent. After that, the purity and the concentration of total RNA were measured by cDNA synthesis kits with an oligo-adaptor primer, and then the total RNA was reverse-transcribed into cDNA. Eventually, the quantitative analysis of the production of cDNA encoding iNOS, TNF-α, and IL-6 was performed by a real-time quantitative PCR instrument (Bio-Rad, CA, U.S.A.). The primer sequences were 5′-AGGGAATCTTGGAGCGAGTT-3′ (forward) and 5′-GCAGCCTCTTGTCTTTGACC-3′ (reverse) for iNOS; 5′-CCACCACGCTCTTCTGTCTACTG-3′ (forward) and 5′-GGGCTACGGGCTTGTCACTC-3′ (reverse) for TNF-α; 5′-TTCCAGCCAGTTGCCTTCTTG-3′ (forward) and 5′-GGTCTGTTGTGGGTGGTATCCTC-3′ for IL-6; and 5′-TGGAATCCTGTGGCATCCATGAAAC-3′ (forward) and 5′-TAAAACGCAGCTCAGTAACAGTCCG-3′ (reverse) for β-actin (the internal reference).

Transcript-metabolite analysis

Transcript analysis

The transcript analysis of the control group and UPP-3 (100 μg/mL) treated macrophage cells was carried out by the previous method (Han et al., 2021). In brief, the control and UPP-3-treated macrophage cells were used to establish the transcript library and Illumina sequencing (3 biological replicates per group). Using the Illumina HiSeq™ 2500 platform (Illumina Inc., San Diego, CA, U.S.A.), the transcript library was paired-end sequenced according to the manufacturer's instructions. The RNA concentration and RNA integrity were carried out on an Agilent 2100 system (Agilent Technologies Inc., Palo Alto, CA, U.S.A.) and a NanoDrop 2000 spectrophotometer (ThermoFisher Scientific, MA, U.S.A.), respectively. The index of the reference genome file was directly downloaded from the public genome website, and paired-end clean reads matched to the reference genome were established via Hisat v2.0.5. High-quality clean reads (clean data) were obtained from the mixed RNA samples of the control group and UPP-3-treated macrophage cells to establish a whole transcript as a reference for further differentially expressed genes (DEGs) analysis.

Metabolite analysis

The metabolite analysis between the control group and UPP-3 (100 μg/mL) treated macrophage cells was determined based on a standard metabolic operating procedure (Han et al., 2021). The differential metabolites of UPP-3-treated macrophage RAW264.7 cells were identified by the public metabolite information database combined with the MetWare (Metware Biotechnology Co., Ltd. Wuhan, China) database. The widely targeted metabolic profile of the extracts (100 μg/mL) of the control and UPP-3-treated macrophage RAW264.7 cell groups were performed by UPLC-ESI-MS/MS system (UPLC, Shim-pack UFLC SHIMADZU CBM A system; MS, QTRAP® System). Orthogonal partial least-squares discriminant analysis (OPLS-DA) and Pareto-scaled principal component analysis (PCA) were applied to further analyze and normalize the obtained metabolic data. Then, the result of OPLS-DA contributed to the classification with the projection (VIP) value. Metabolites were considered differently accumulated metabolites (DAMs) with the VIP-value > 1 and p-values < 0.05.

Bioinformatic analysis

The analysis of Kyoto Encyclopedia of Genes and Genomes (KEGG) pathways was carried out via a Blast2GO. Only the pathways with p-values < 0.05 were considered significant.

Western blot analysis

For UPP-3 western blots, 2×10^6 cells in six-well plates were cultured. Cells in 1 × Cell Lysis buffer were lysed (Cell Signaling Technologies, MA, U.S.A.) that contained 20 mM Tris-HCl pH 7.5, 150 mM NaCl, 1 mM EGTA, 1 mM EDTA, 1% Triton, 1 mM β-glycerophosphate, 2.5 mM sodium pyrophosphate, 1 mM Na_3VO_4, 1 μg/mL leupeptin, supplemented with the HALT protease and phosphatase inhibitor cocktail (ThermoFisher Scientific, MA, U.S.A.) (Rothenberg, Yang, Chen, Zhang & Zhang, 2019). A total of 30 μg protein was electrophoresed per lane on a 4–12% Bis-Tris SDS-PAGE gel. Electrophoresed gels soaked in 2 × NuPage Transfer buffer (ThermoFisher Scientific, MA, U.S.A.) and 10% methanol were gently shaken for 15 min. Proteins were transferred to nitrocellulose membranes (ThermoFisher Scientific, MA, U.S.A.) via the iBlot detection and transfer system (ThermoFisher Scientific, MA, U.S.A.). Membranes with the primary antibody solutions were incubated in 4% milk dissolved in 1 × TBST at room temperature for 1 h. The membranes were cultured at 4 °C overnight, including GAPDH, TLR-4, NF-κB p65 (Amersham Life Science, Amersham, England), and further incubated with anti-rabbit antibodies conjugated to horseradish phosphatase for 1 h at room temperature. After 30 min wash in 1 × TBST at room temperature, the blots were developed via enhanced chemiluminescence (Amersham Life Science, Amersham, England).

Immunofluorescent staining

RAW264.7 cells fixed with 4% paraformaldehyde for 20 min at 4 °C were incubated in 0.5% Triton for 15 min. After blocking the cells with 5% goat serum at room temperature for 30 min, the cells were later incubated with the primary antibodies (anti-NF-κB p65) at 4 °C for 24 h. After washing 3 times with PBS, DAPI was applied to stain the nucleus, samples were cultured with fluorescence conjugated secondary antibody at room temperature for 1 h. After being removed with PBS, the cells were stained with DAPI at 1:1000 for 10 min. Coverslips were mounted with fluorescent mounting medium. Images were acquired by a Cytation 5 cell imaging multi-mode reader (Olympus SpinSR10 spinning disk confocal super-resolution microscope).

Statistical analysis

All the measurements were carried out in triplicate or sextuplicate. All the obtained data were expressed as mean ± standard deviations (SD). The statistical analyses were measured using ANOVA (SPSS 20.0). A significant statistical significance was defined with a p-value of < 0.05 or 0.01.

Results and discussion

Preparation and structural characterization

The *U. pinnatifida* polysaccharide (UPP) was obtained based on a conventional method with the main process of hot water extraction, alcohol precipitation, and deproteinization. The UPP yield was about 3.80 ± 0.03%. The UPP was chromatographed on a DEAE ion-exchange chromatographic column to yield UPPs 1–3 illustrated in Fig. 1a. UPPs 1–3 were sequentially subjected to Sephadex G-100 size-exclusion chromatographic column, respectively, to gain a well-proportioned peak (Fig. 1c). The yield of UPP 1–3 was about 10.5 ± 0.05%, 9% ± 0.12%, and 19.75 ± 1.69%, compared with crude polysaccharides from

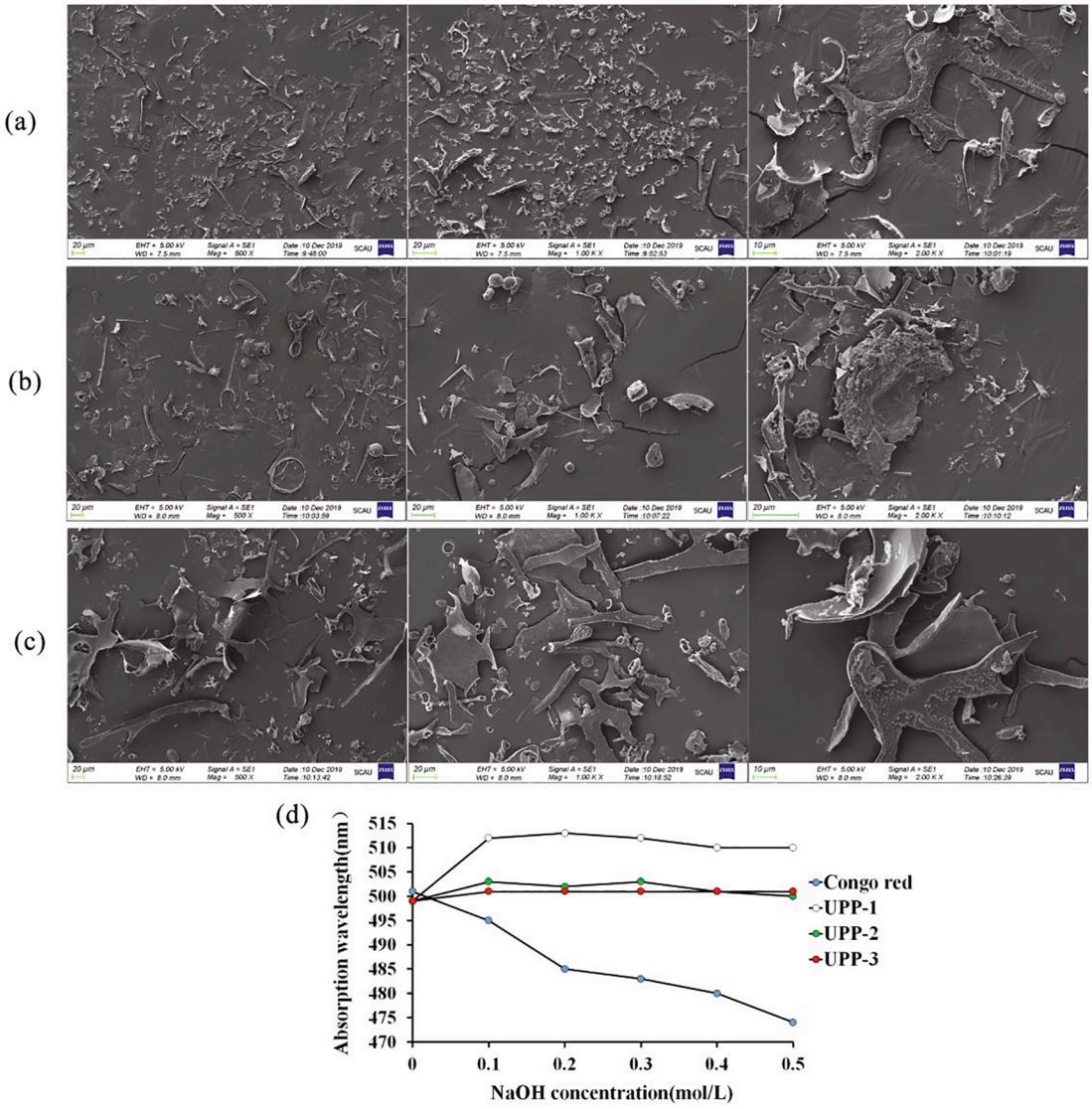

Fig. 2. (a-c) The SEM morphological properties of UPP-1 (a), UPP-2 (b), UPP-3(c). (d) The triple-helix conformation analysis of UPPs 1–3.

U. pinnatifida.

The analysis of primary characteristic of UPPs 1–3 revealed the total sugar contents of 56.0 ± 0.21%, 41.4 ± 0.11%, and 79.4 ± 0.15%, the uronic acid contents of 29 ± 0.05%, 12.0 ± 0.08%, and 10.0 ± 0.09%, the total protein contents of 0.09 ± 0.08%, 0.29 ± 0.12%, and 0.17 ± 0.05%, and the sulfate contents of 9.17 ± 0.09%, 10.0 ± 0.05%, and 15.0 ± 6.56%, respectively.

The average MWs of UPPs were homogeneous polysaccharides with different MWs of 7.212 kDa, 13.924 kDa, and 55.875 kDa, respectively (Fig. 1d). UPPs 1–3 were polysaccharides confirmed by polysaccharide absorption at 199 nm for polysaccharide UV absorption and weak protein characteristic absorption at 280 and 260 nm (Fig. 1e) for the minor contents of the protein of UPPs 1–3 (Rothenberg et al., 2019). As shown in Fig. 1b, UPPs 1–3 were composed of galactose, glucose, xylose, mannose, glucuronic acid, and mannuronic acid (99.08%, 99.20%, and 3.52%, respectively). In comparison, UPP-3 also consisted of fucose (31.51%), arabinose (0.60%), and fructose (0.63%), which indicated that mannuronic acid might be the prominent sugar residues of UPPs 1 and 2. In contrast, fucose and glucuronic acid might be domained in the UPP-3. Thus, the UPPs 1–3 are all heteropolysaccharides.

The FT-IR spectra (Fig. 1f), UPPs 1–3 showed typical signals of sulfated polysaccharides assigned in line with those reported data (Chen et al., 2017). The broadbands at 3400 cm^{-1} (O—H stretching vibration), 2932 cm^{-1} (C—H stretching), 1415 cm^{-1} (C—H bending vibration), 1606 cm^{-1} for the uronic acid signal (C—H stretching vibration of C═O), 1300 cm^{-1} (O═S = O stretching vibration) (Zhang et al., 2019) and 820 cm^{-1} (C—O—S vibration) (Foley, Szegezdi, Mulloy, Samali & Tuohy, 2011) were identified. The results of these analyses indicated that UPPs were sulfated polysaccharides. In addition, broadbands at the 1033–1257 cm^{-1} for C-OH stretching vibrations and C—O—C glycosidic band vibration were prominent in the region of particular polysaccharides (Zheng et al., 2014).

The morphological characteristic of UPPs was carried out by SEM with magnifications of 500 ×, 1000 ×, and 2000 ×, respectively (Fig. 2a-c). The results illustrated that the fragmentation of UPP-1 and UPP-2 suggested that the binding was not close enough, and the molecular interaction is weak. UPP-3 was lamellar, showed a close connection and strong intermolecular interaction. After mixing with Congo red, there was no significant difference in the maximum absorption wavelength between the Congo red solution of UPPs 1–3 and the pure Congo red solution (Fig. 2d). Therefore, these polysaccharides did not possess triple-helix structures.

Immunomodulatory assay macrophages RAW264.7 cell lines

The cytotoxicity of UPPs on macrophages RAW264.7 cell lines was

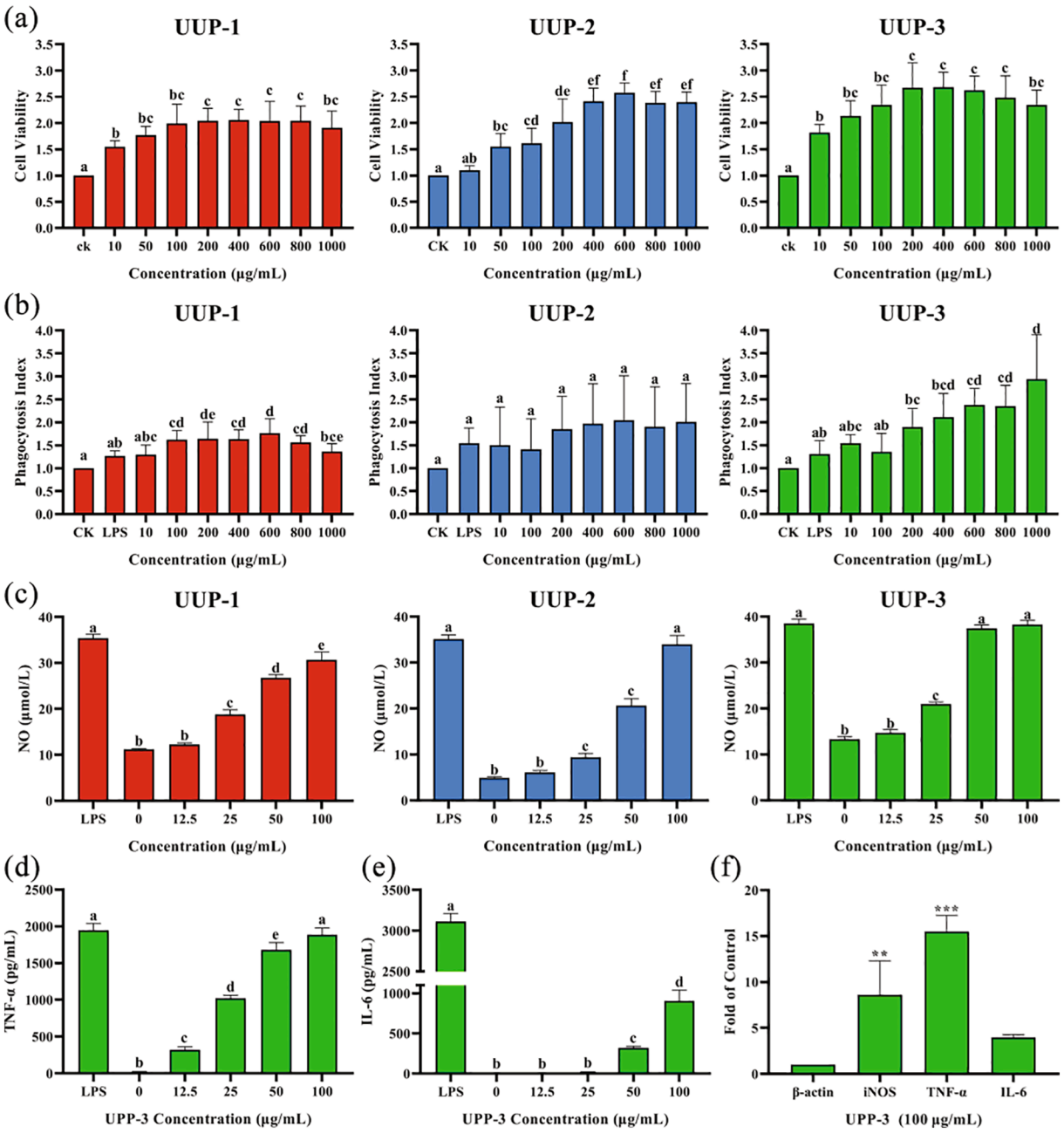

Fig. 3. (a) The proliferation of the macrophage RAW264.7 cells treated with UPPs 1–3 vs. the control group. (b) The phagocytosis of macrophage RAW264.7 cells treated with UPPs 1–3. (c) The NO production of the macrophage RAW264.7 cells treated with UPPs 1–3. (d-e) The secretion of TNF-α (d), IL-6 (e) in macrophage RAW264.7 cells treated with UPP-3. (f) The mRNA expression levels of iNOS, TNF-α, and IL-6 in macrophage RAW264.7 cells treated with UPP-3. The different letters indicate statistically significant differences for each group ($p < 0.05$). ** $p < 0.01$, and *** $p < 0.001$.

assessed based on the CCK-8 method. The results of the cytotoxicity assay (Fig. 3a) indicated that the activity of macrophages incubated with UPPs at a concentration ranging from 10 to 1000 μg/mL was in good growth, indicating UPPs 1–3 had no toxic effects on the macrophages RAW264.7 cells compared with the control group (Wang, Zhang, Shao, Ren, Jia & Li, 2019). UPPs 1–3 could enhance the phagocytosis of macrophage RAW264.7 cells at a concentration ranging from 200 to 800 μg/mL in a rising tendency (Fig. 3b), and also UPP-3 at the concentrations 1000 μg/mL promoted the phagocytosis of macrophages RAW264.7 cell lines, indicated that UPPs could enhance cell phagocytosis of macrophages RAW264.7 cell lines.

NO is known as a vital active substance related to immunomodulating response to macrophage cells (Liu et al., 2017). The NO production of macrophage RAW264.7 cells treated with UPPs 1–3 (Fig. 3c) indicated that UPP-3 showed a better effect of dose-dependent manner than UPPs 1 and 2 in the range of 10 to 100 μg/mL. Therefore, the release of cytokine (TNF-α and IL-6) from macrophage RAW264.7 cells treated with UPP-3 was further evaluated according to the ELISA method. ELISA results (Fig. 3d) displayed that UPP-3 with a dose-dependent increasing tendency ranging from 12.5 to 100 μg/mL could significantly induce macrophage RAW264.7 cells to secret TNF-α. In addition, UPP-3 could significantly induce the secretion of IL-6 in macrophage RAW264.7 cells. The molecular details of regulatory mechanisms of the UPP-3-treated RAW264.7 macrophage cells need further investigation.

To investigate whether the enhancement of NO, IL-6, and TNF-α relate to their gene expressions, the mRNA expression levels of iNOS, IL-6, and TNF-α in macrophage RAW264.7 cells affected by UPP-3 were

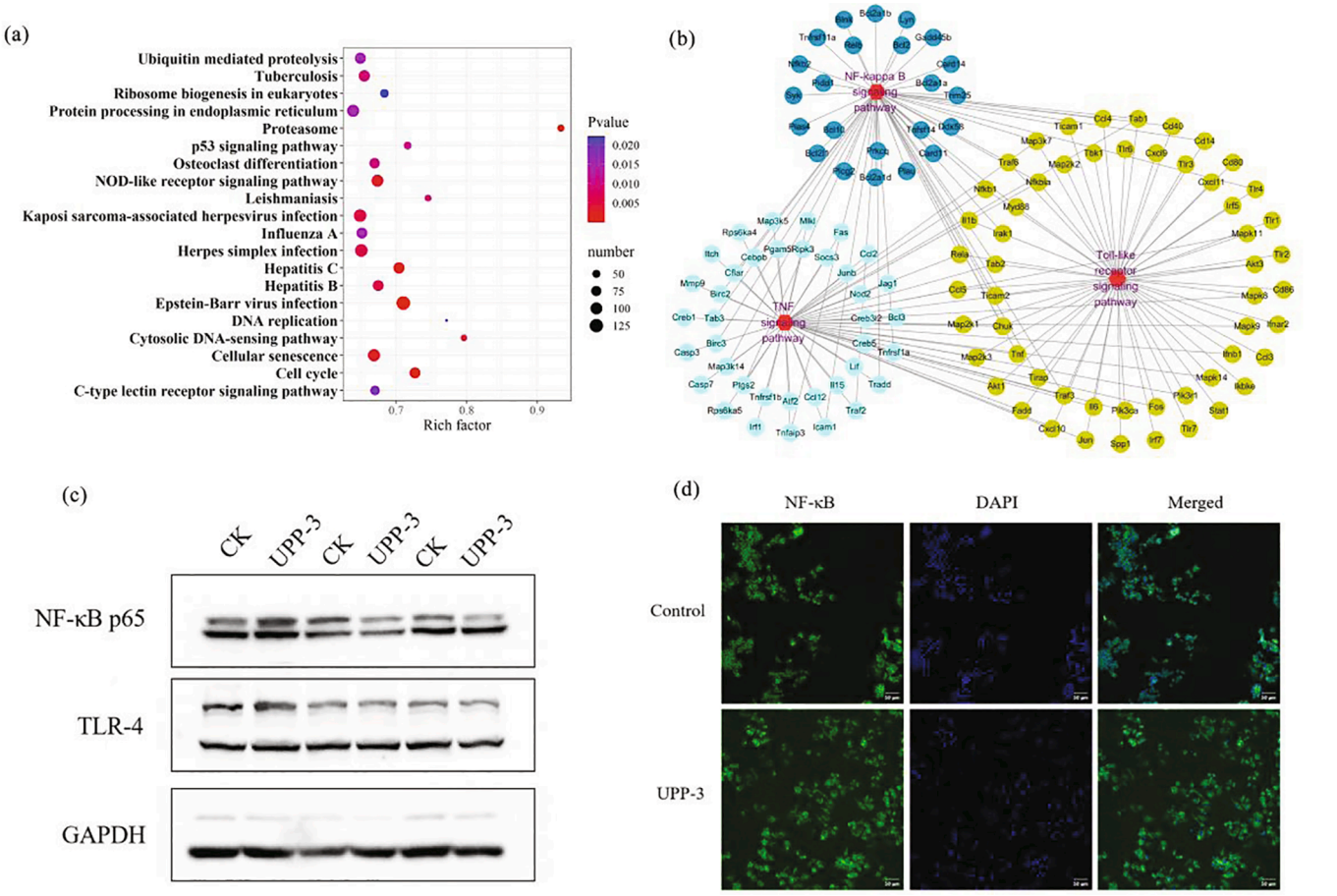

Fig. 4. (a) The KEGG pathway enrichment analysis of DEGs. (b) Genes of the topical immunomodulating signaling pathways in the macrophage RAW264.7 cells treated with UPP-3. (c) Measurement of NF-κB p65 and TLR-4 in macrophages by western blot. GAPDH was used as an equal loading control. (d) Translocation of the anti-NF-κB p65 from the cytoplasm into the nucleus was evaluated by immunofluorescent staining.

determined based on the RT-qPCR method. As is demonstrated in Fig. 3d-f, compared to those of the control group, UPP-3 in a dose-dependent manner could significantly enhance the expression levels of iNOS, TNF-α, and IL-6. Compared with the control group, the mRNA expression levels of iNOS and TNF-α of the macrophage RAW264.7 cells treated with UPP-3 (100 μg/mL) were significantly increased, while the mRNA expression level of IL-6 was not significantly affected. In general, the gene expression of NO and cytokines (IL-6 and TNF-α) were regulated by the NF-κB transcription factors (Huang et al., 2020). These results revealed that UPP-3 could stimulate the levels of NO, IL-6, and TNF-α through regulating the gene expression of iNOS, IL-6, and TNF-α in macrophage RAW264.7 cells.

Transcript-metabolite analysis of the macrophages RAW264.7 cells treated with UPP-3

Transcript analysis of macrophages RAW264.7 cells treated with UPP-3

DEGs between the control and the UPP-3-treated groups were defined as variable importance in the project (VIP) ≥ 1 with a fold change ≥ 2 or a fold change ≤ 0.5. The transcriptome analysis revealed that 3970 up-regulated DEGs and 3865 down-regulated DEGs of the total 7835 DEGs between the control and UPP-3-treated macrophage RAW264.7 cell groups. The functional annotation of DEGs between the control and UPP-3-treated macrophage RAW264.7 cell groups was performed according to the KEGG database. The KEGG enrichment analysis revealed twenty significantly enriched pathways in the macrophages RAW264.7 cells treated with UPP-3. In contrast, the terms associated with the topical immunomodulatory signaling pathways, such as "Toll-like receptor" (Yang et al., 2018), "TNF" (Tabarsa, You, Yelithao, Palanisamy, Prabhu & Nan, 2020), and "NF-kappa B" (Tabarsa, You, Abedi, Ahmadian, Li & Talapphet, 2019) signaling pathways were not enriched (Fig. 4a-b, and Table S3). To investigate the molecular details of the macrophages RAW264.7 cells treated with UPP-3 (Fig. 4c-d), the protein expressions of NF-κB p65 and TLR-4 in the macrophages RAW264.7 cells treated with UPP-3 were performed by Western blot. TLR4 is a significant membrane protein receptor for recognizing lipopolysaccharides (LPS) from Gram-negative bacteria and involves the body's immune response. NF-κB signaling pathways significantly get involved in the inflammatory reaction, apoptosis, and immune responses in RAW264.7 macrophages. UPP-3 could down-regulate the protein TLR-4 expressions and induce the translocation of NF-κB p65 into the nucleus in macrophage cells, indicating UPP-3 could activate macrophage RAW264.7 cells *via* the TLR-4 and NF-κB p65 signaling pathways.

Metabolite analysis

The obtained metabolite data of the macrophage RAW264.7 cells treated with UPP-3 vs. the control group were verified by the essential spectrum of quality (Fig. S2) and the obtained metabolite data were subjected to PCA analysis. The PCA score plots displayed a high separation resolution between the UPP-3-treated and the control groups (Fig. S3). The OPLS-DA analysis indicated that the prominent bioactive metabolites between the control and UPP-3-treated macrophage RAW264.7 cell groups were significantly changed (Fig. S4-S6). The DAMs between the control and UPP-3-treated macrophage RAW264.7 cell groups were considered as variable importance in the project (VIP)

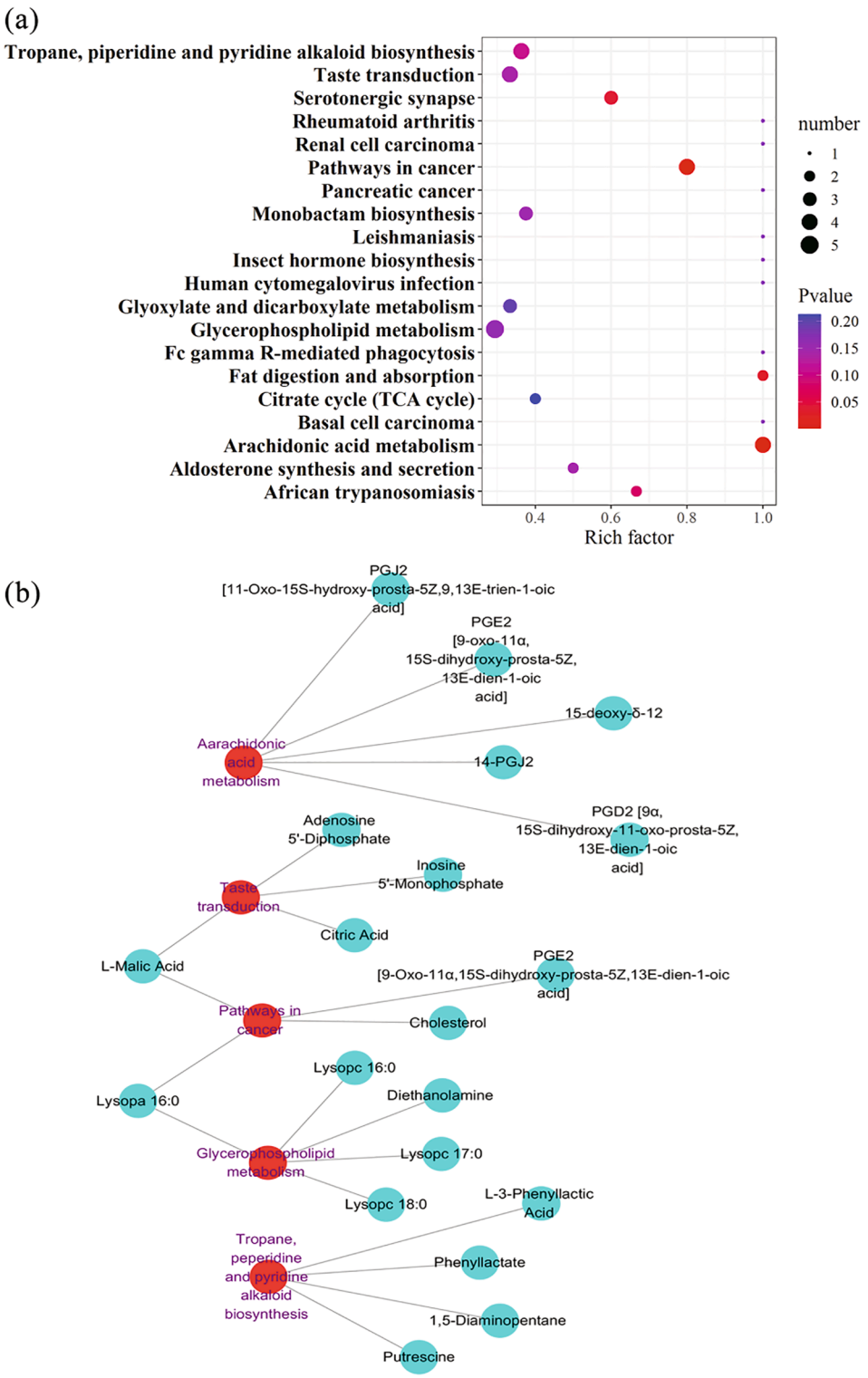

Fig. 5. (a) The enrichment KEGG pathway analysis of DAMs. (b) Five DAMs related to functionally annotated pathways in the macrophages RAW264.7 treated with UPP-3. (c) The KEGG pathway enrichment analysis of DEGs. (d) Genes of the topical immunomodulating signaling pathways in the macrophage RAW264.7 cells treated with UPP-3.

≥ 1 with a fold change ≥ 2 or a fold change ≤ 0.5 (Fig. S7, Fig. S8, and Table S1). The metabolome analysis (Table S1) revealed 43 up-regulated DAMs and 29 down-regulated DAMs of the 72 DAMs between the UPP-3-treated and the control groups. DAMs between the control and UPP-3-treated macrophage RAW264.7 cell groups were functionally annotated according to the public KEGG database. The enrichment analysis of KEGG showed that five terms "glycerophospholipid metabolism", "arachidonic acid metabolism", "tropane, peperidine and pyridine alkaloid biosynthesis", "taste transduction", and "pathways in cancer" were significantly enriched (Fig. 5a). Five DAMs are associated with the pathway of glycerophospholipid metabolism. Four DAMs are linked with the pathway of arachidonic acid metabolism. Four DAMs are linked

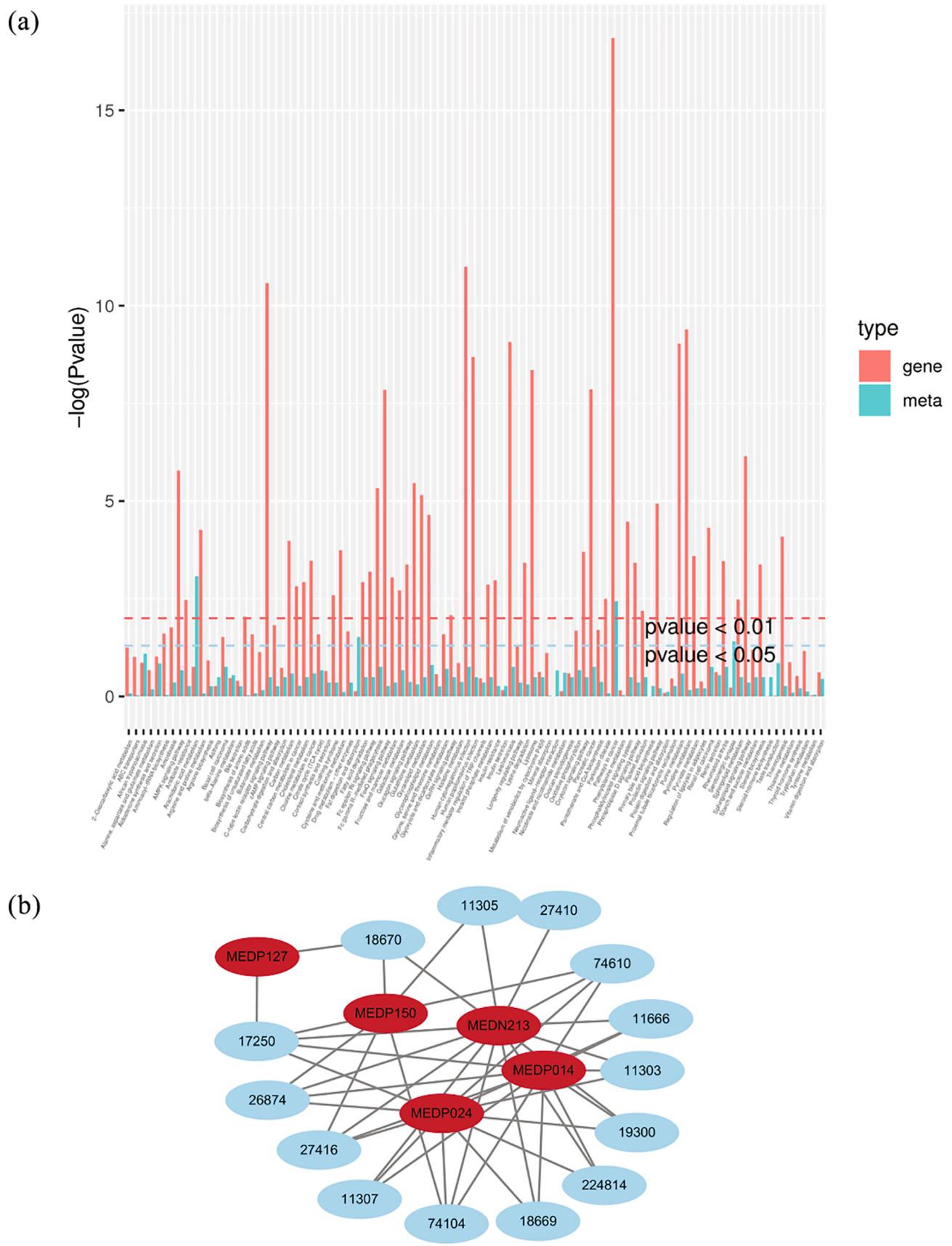

Fig. 6. (a) DAMs and DEGs of the macrophages RAW264.7 treated with UPP-3 are both involved in KEGG pathways. (b) The correlation network of DAMs and DEGs in the macrophage RAW264.7 cells treated with UPP-3.

to the pathway of tropane, peperidine, and pyridine alkaloid biosynthesis. Four DAMs are associated with the taste transduction pathway. Four DAMs are related to the pathways in cancer. These data are illustrated in Fig. 5b and Table S2. Some of these pathways were involved in the inflammation of drug-stimulated RAW264.7 macrophages (Tsai et al., 2018). These pathways of glycerophospholipid metabolism, arachidonic acid metabolism, tropane, peperidine, and pyridine alkaloid biosynthesis, taste transduction, and pathways in cancer were enriched in the macrophage RAW264.7 cells treated with UPP-3 indicated that UPP-3 might affect the five significant signaling pathways of macrophage RAW264.7 cells.

Transcript-metabolite analysis of the macrophage RAW264.7 cell treated with UPP-3

To analyze the properties of DAMs and DEGs enriched in the macrophage RAW264.7 cell treated with UPP-3, the correlation network was established. In our present investigation, correlation pairs associated with the functionally annotated signaling pathways were included (Fig. 6a). The visualized network showed the DAMs connected to the corresponding DEGs (Fig. 6b and Table S4). Four DAMs between the UPP-3-treated and the control groups got involved in the pathways in cancer as illustrated in Fig. 6b and Table S2, which suggested that UPP-3 could activate macrophage RAW264.7 cells *via* the TLR-4 and NF-κB p65 pathways.

Previous researches have illustrated that the immune-regulatory effects of polysaccharides are associated with their structural characteristics, such as molecular weights, monosaccharide composition, the type of glycosidic linkages, branching characteristics, functional groups, and triple-helix conformation (Li, Dong, Zhang, Huang, Liu & Fu, 2020). The molecular weights of polysaccharides and their molecular weight distributions are usually closely linked to the biological properties of polysaccharides (Zhang et al., 2020). Our present investigation indicated that UPPs 1–3 were homogeneous polysaccharides with different MWs of 7.212 kDa (UPP-1), 13.924 kDa (UPP-2), and 55.875 kDa (UPP-3), respectively, and the three fractional polysaccharides showed significant immune-regulatory effects, and UPP-3 (Mw = 55.875 kDa) exhibited better macrophage-activating activity than that of UPPs 1–2. Additionally, the sulfate contents of polysaccharides had significantly responsible for the resulting immune-stimulatory effects (Yelithao, Surayot, Park, Lee, Lee & You, 2019). In the current report, UPPs 1–3 consisted of sulfate contents of 9.17 ± 0.09%, 10.0 ± 0.05%, and 15.0 ± 6.56%, respectively, and they displayed significant effects on macrophage RAW264.7 cells, while UPP-3 with a more sulfate content (15.0 ± 6.56%) possess better macrophage-activating effect than that of UPPs 1–2. In our present study, the MWs, the sulfate contents, UPPs 1–3 showed different contents, and ratios of the monosaccharide composition from those species in previous reports (Han et al., 2019). This suggested that the primary structural characterization of the obtained polysaccharides should be further investigated. Besides, the morphological characteristic of UPPs 1–3 could give a supplement to the structural characterization of *U. pinnatifida* polysaccharides. More interesting, although the gene expression of NO and cytokines (IL-6 and TNF-α) were down-regulated, the protein expressions of TLR-4 were up-regulated *via* the NF-κB transcription factors. These transcript-metabolite data indicated that the terms linked with the significant immunomodulatory signaling pathways, such as "Toll-like receptor" (Yang et al., 2018), "TNF" (Tabarsa et al., 2020), and "NF-κB" (Tabarsa et al., 2019) signaling pathways, were not enriched. However, the co-mapped correlation network of transcript-metabolite combined with western blot and immunofluorescent staining indicated that UPP-3 could activate TLR4 involved in NF-κB p65 signaling pathway to drive immunomodulatory phenotype. Besides, four DAMs in between the UPP-3-treated and the control groups got involved in the pathways in cancer illustrated in Fig. 4d and Table S2, which indicated that UPP-3 might show a significant effect on the macrophage RAW264.7 via another new signaling pathway, and also give a new sight into its antitumor activity (Tabarsa et al., 2019).

Conclusions

In summary, our present investigation focused on the structural characterization, immunostimulating effects, and the transcriptome-metabolome analysis of the sulfated *U. pinnatifida* polysaccharides (UPPs 1–3). All UPPs 1–3 were composed of galactose, xylose, mannose, glucose, glucuronic acid, and mannuronic acid, while UPP-3 also consisted of fucose, arabinose, and fructose. UPPs 1–3 showed different SEM morphological properties and had molecular weights of 7.212 kDa, 13.924 kDa, and 55.875 kDa, with sulfate contents of 9.17 ± 0.09%, 10 ± 0.05%, and 15 ± 0.17%, respectively. Among these three fractional polysaccharides, UPP-3 showed a better effect on the phagocytic activity of macrophages RAW264.7, level of nitric oxide, and mRNA expression of cytokines (iNOS, TNF-α, and IL-6) than those of UPPs 1–2. UPP-3 could activate macrophages RAW264.7 *via* the TLR-4 and NF-κB p65 pathways. The transcriptome and metabolome analysis demonstrated 3970 up-regulated DEGs and 3865 down-regulated DEGs of the total 7835 DEGs, 43 up-regulated DAMs, and 29 down-regulated DAMs of the 72 DAMs in the macrophage RAW264.7 treated with UPP-3. The combined analysis of transcriptome and metabolome with Western blot and immunofluorescent staining indicated that UPP-3 could activate TLR4 receptors involved in NF-κB p65 signaling pathway to drive the immunomodulatory phenotype. Besides, a series of potential metabolites in the macrophage RAW264.7 treated with UPP-3 were identified, which might provide valuable scientific data for a detailed investigation of the immune-stimulatory *U. pinnatifida* sulfated polysaccharides. Thus, these findings will provide valuable scientific data including structural characterization, cytokines of immune-stimulatory effects, and molecular details of transcription and metabolism for an in-depth investigation of the regulatory mechanism of *U. pinnatifida* sulfated polysaccharides.

Declaration of Competing Interest

The authors declare that they have no known competing financial interests or personal relationships that could have appeared to influence the work reported in this paper.

Acknowledgments

This work was financially supported by the Key-Area Research and Development Program of Guangdong Province (No. 2020B1111030004), the National Natural Science Foundation of China (No. 32161160304), Program of Department of Natural Resources of Guangdong Province (No. GDNRC[2020]038 and GDNRC[2021]53), Guangdong Provincial Key Laboratory of Aquatic Product Processing and Safety (No. GDPKLAPPS2102), and Guangdong Provincial Key Laboratory of Food Quality and Safety (No. 2020B1212060059).

Appendix A. Supplementary data

Supplementary data to this article can be found online at https://doi.org/10.1016/j.fochx.2022.100251.

References

Adrien, A., Bonnet, A., Dufour, D., Baudouin, S., Maugard, T., & Bridiau, N. (2019). Anticoagulant activity of sulfated ulvan isolated from the green macroalga *Ulva rigida*. *Marine Drugs, 17*(5), 291.

Bovet, L., Samer, C., & Daali, Y. (2019). Preclinical evaluation of safety of fucoidan extracts from *Undaria pinnatifida* and *Fucus vesiculosus* for use in cancer treatment. *Integrative Cancer Therapies, 18*, 1871094757.

Bradford, M. M. (1976). A rapid and sensitive method for the quantitation of microgram quantities of protein utilizing the principle of protein-dye binding. *Analytical Biochemistry, 72*(1-2), 248–254.

Cao, C., Huang, Q., Zhang, B., Li, C., & Fu, X. (2018). Physicochemical characterization and in vitro hypoglycemic activities of polysaccharides from *Sargassum pallidum* by

microwave-assisted aqueous two-phase extraction. *International Journal of Biological Macromolecules, 109*, 357–368.
Chen, Z.-E., Wufuer, R., Ji, J.-H., Li, J.-F., Cheng, Y.-F., Dong, C.-X., & Taoerdahong, H. (2017). Structural characterization and immunostimulatory activity of polysaccharides from *Brassica rapa* L. *J Agric Food Chem, 65*(44), 9685–9692.
Dodgson, K. S., & Price, R. G. (1962). A note on the determination of the ester sulphate content of sulphated polysaccharides. *Biochemical Journal, 84*, 106–110.
Foley, S. A., Szegezdi, E., Mulloy, B., Samali, A., & Tuohy, M. G. (2011). An unfractionated fucoidan from *Ascophyllum nodosum*: Extraction, characterization, and apoptotic effects in vitro. *Journal of Natural Products, 74*(9), 1851–1861.
Gao, X., Qu, H., Gao, Z., Zeng, D., Wang, J., Baranenko, D., … Lu, W. (2019). Protective effects of *Ulva pertusa* polysaccharide and polysaccharideiron (III) complex on cyclophosphamide induced immunosuppression in mice. *International Journal of Biological Macromolecules, 133*, 911–919.
Gao, X., Qu, H., Shan, S., Song, C., Baranenko, D., Li, Y., & Lu, W. (2020). A novel polysaccharide isolated from *Ulva pertusa:* Structure and physicochemical property. *Carbohydrate Polymers, 233*, 115849. https://doi.org/10.1016/j.carbpol.2020.115849
Gurpilhares, D.d. B., Cinelli, L. P., Simas, N. K., Pessoa Jr., A., & Sette, L. D. (2019). Marine prebiotics: Polysaccharides and oligosaccharides obtained by using microbial enzymes. *Food Chemistry, 280*, 175–186.
Han, Y.u., Hao, H., Yang, L., Chen, G., Wen, Y., & Huang, R. (2019). Nutritional characteristics of marine fish *Sardinella zunasi* Bleeker and immunostimulatory activities of its glycoprotein. *RSC Advances, 9*(52), 30144–30153.
Han, Y.u., Wu, Y., Li, G., Li, M., Yan, R.u., Xu, Z., … Huang, R. (2021). Structural characterization and transcript-metabolite correlation network of immunostimulatory effects of sulfated polysaccharides from green alga *Ulva pertusa*. *Food Chemistry, 342*, 128537. https://doi.org/10.1016/j.foodchem.2020.128537
Hao, H., Han, Y.u., Yang, L., Hu, L., Duan, X., Yang, X., & Huang, R. (2019). Structural characterization and immunostimulatory activity of a novel polysaccharide from green alga *Caulerpa racemosa* var *peltata*. *International Journal of Biological Macromolecules, 134*, 891–900.
Huang, Z., Zeng, Y.-J., Chen, X.i., Luo, S.-Y., Pu, L., Li, F.-Z., … Lou, W.-Y. (2020). A novel polysaccharide from the roots of *Millettia Speciosa* Champ: Preparation, structural characterization and immunomodulatory activity. *International Journal of Biological Macromolecules, 145*, 547–557.
Koh, H. S. A., Lu, J., & Zhou, W. (2019). Structure characterization and antioxidant activity of fucoidan isolated from *Undaria pinnatifida* grown in New Zealand. *Carbohydrate Polymers, 212*, 178–185.
Lee, J.-B., Hayashi, K., Hashimoto, M., Nakano, T., & Hayashi, T. (2004). Novel antiviral fucoidan from sporophyll of *Undaria pinnatifida* (Mekabu). *Chemical & Pharmaceutical Bulletin (Tokyo), 52*(9), 1091–1094.
Li, C., Dong, Z., Zhang, B., Huang, Q., Liu, G., & Fu, X. (2020). Structural characterization and immune enhancement activity of a novel polysaccharide from *Moringa oleifera* leaves. *Carbohydrate Polymers, 234*, 115897. https://doi.org/10.1016/j.carbpol.2020.115897
Liu, X., Xie, J., Jia, S., Huang, L., Wang, Z., Li, C., & Xie, M. (2017). Immunomodulatory effects of an acetylated *Cyclocarya paliurus* polysaccharide on murine macrophages RAW264.7. *International Journal of Biological Macromolecules, 98*, 576–581.
Masuko, T., Minami, A., Iwasaki, N., Majima, T., Nishimura, S.-I., & Lee, Y. C. (2005). Carbohydrate analysis by a phenol-sulfuric acid method in microplate format. *Analytical Biochemistry, 339*(1), 69–72.
Gudiel-Urbano, M., & Goñi, I. (2002). Effect of edible seaweeds (*Undaria pinnatifida* and *Porphyra ternera*) on the metabolic activities of intestinal microflora in rats. *Nutrition Research, 22*(3), 323–331. https://doi.org/10.1016/S0271-5317(01)00383-9
Qiu, S.-M., Aweya, J. J., Liu, X., Liu, Y., Tang, S., Zhang, W., & Cheong, K.-L. (2022). Bioactive polysaccharides from red seaweed as potent food supplements: A systematic review of their extraction, purification, and biological activities. *Carbohydrate Polymers, 275*, 118696. https://doi.org/10.1016/j.carbpol.2021.118696
Raguraman, V., L, S. A., J, J., Palaniappan, S., Gopal, S., R, T., & R, K. (2019). Sulfated polysaccharide from *Sargassum tenerrimum* attenuates oxidative stress induced reactive oxygen species production in in vitro and in zebrafish model. *Carbohydrate Polymers, 203*, 441–449.
Rothenberg, D. O., Yang, H., Chen, M., Zhang, W., & Zhang, L. (2019). Metabolome and transcriptome sequencing analysis reveals anthocyanin metabolism in pink flowers of anthocyanin-rich tea (*Camellia sinensis*). *Molecules, 24*(6), 1064.
Sim, S.-Y., Shin, Y.-E., & Kim, H.-K. (2019). Fucoidan from *Undaria pinnatifida* has anti-diabetic effects by stimulation of glucose uptake and reduction of basal lipolysis in 3T3-L1 adipocytes. *Nutrition Research, 65*, 54–62.
Sun, Q.-L., Li, Y.i., Ni, L.-Q., Li, Y.-X., Cui, Y.-S., Jiang, S.-L., … Dong, C.-X. (2020). Structural characterization and antiviral activity of two fucoidans from the brown algae *Sargassum henslowianum*. *Carbohydrate Polymers, 229*, 115487. https://doi.org/10.1016/j.carbpol.2019.115487
Tabarsa, M., You, SangGuan, Abedi, M., Ahmadian, N., Li, C., & Talapphet, N. (2019). The activation of RAW264.7 murine macrophage and natural killer cells by glucomannogalactan polysaccharides from *Tornabea scutellifera*. *Carbohydrate Polymers, 219*, 368–377.
Tabarsa, M., You, SangGuan, Yelithao, K., Palanisamy, S., Prabhu, N. M., & Nan, M.a. (2020). Isolation, structural elucidation and immuno-stimulatory properties of polysaccharides from *Cuminum cyminum*. *Carbohydrate Polymers, 230*, 115636. https://doi.org/10.1016/j.carbpol.2019.115636
Tong, D., Guijie, C., Yi, S., Shiyi, O., Xiaoxiong, Z., & Hong, Y. (2017). Antioxidant and immunostimulating activities in vitro of sulfated polysaccharides isolated from *Gracilaria rubra*. *Journal of Functional Foods, 28*.
Tsai, P.-J., Huang, W.-C., Lin, S.-W., Chen, S.-N., Shen, H.-J., Chang, H., & Chuang, L.-T. (2018). Juniperonic acid incorporation into the phospholipids of murine macrophage cells modulates pro-inflammatory mediator production. *Inflammation, 41*(4), 1200–1214.
Usoltseva, R. V., Anastyuk, S. D., Ishina, I. A., Isakov, V. V., Zvyagintseva, T. N., Thinh, P. D., … Ermakova, S. P. (2018). Structural characteristics and anticancer activity in vitro of fucoidan from brown alga *Padina boryana*. *Carbohydrate Polymers, 184*, 260–268.
Wang, L., Park, Y.-J., Jeon, Y.-J., & Ryu, B. (2018). Bioactivities of the edible brown seaweed, *Undaria pinnatifida* : A review. *Aquaculture, 495*, 873–880.
Wang, P., Liu, Z., Liu, X., Teng, H., Zhang, C., Hou, L., … Singh, S. (2014). Anti-metastasis effect of fucoidan from *Undaria pinnatifida* sporophylls in mouse hepatocarcinoma Hca-F cells. *PLoS One, 9*(8), e106071.
Wang, Y., Zhang, Y., Shao, J., Ren, X., Jia, J., & Li, B. (2019). Study on the immunomodulatory activity of a novel polysaccharide from the lichen *Umbilicaria Esculenta*. *International Journal of Biological Macromolecules, 121*, 846–851.
Xu, S. Y., Huang, X., & Cheong, K. L. (2017). Recent advances in marine algae polysaccharides: Isolation, structure, and activities. *Marine Drugs, 15*(12), 388.
Yang, Y., Zhao, X., Li, J., Jiang, H., Shan, X., Wang, Y., … Yu, G. (2018). A beta-glucan from *Durvillaea Antarctica* has immunomodulatory effects on RAW264.7 macrophages via toll-like receptor 4. *Carbohydrate Polymers, 191*, 255–265.
Yelithao, K., Surayot, U., Park, WooJung, Lee, SangMin, Lee, D.-H., & You, SangGuan (2019). Effect of sulfation and partial hydrolysis of polysaccharides from *Polygonatum sibiricum* on immune-enhancement. *International Journal of Biological Macromolecules, 122*, 10–18.
Yu, Y., Zhang, Y., Hu, C., Zou, X., Lin, Y., Xia, Y., & You, L. (2019). Chemistry and immunostimulatory activity of a polysaccharide from *Undaria pinnatifida*. *Food and Chemical Toxicology, 128*, 119–128.
Zhang, S., An, L., Li, Z., Wang, H., Shi, L., Zhang, J., … Guo, Y. (2020). An active heteropolysaccharide from the rinds of *Garcinia mangostana* Linn.: Structural characterization and immunomodulation activity evaluation. *Carbohydrate Polymers, 235*, Article 115929.
Zhang, Z., Wang, H., Chen, T., Zhang, H., Liang, J., Kong, W., … Wang, J. (2019). Synthesis and structure characterization of sulfated galactomannan from fenugreek gum. *International Journal of Biological Macromolecules, 125*, 1184–1191.
Zheng, W., Zhao, T., Feng, W., Wang, W., Zou, Y.e., Zheng, D., … Wu, X. (2014). Purification, characterization and immunomodulating activity of a polysaccharide from flowers of *Abelmoschus esculentus*. *Carbohydrate Polymers, 106*, 335–342.